Geometric Origin of Non-Bloch $\mathcal{PT}$ Symmetry Breaking

Yu-Min Hu,[1] Hong-Yi Wang,[1] Zhong Wang,[1] and Fei Song[1,2,*]
[1]Institute for Advanced Study, Tsinghua University, Beijing, 100084, China
[2]Kavli Institute for Theoretical Sciences, Chinese Academy of Sciences, Beijing, 100190, China

(Received 2 February 2023; revised 5 November 2023; accepted 3 January 2024; published 31 January 2024)

The parity-time ($\mathcal{PT}$) symmetry of a non-Hermitian Hamiltonian leads to real (complex) energy spectrum when the non-Hermiticity is below (above) a threshold. Recently, it has been demonstrated that the non-Hermitian skin effect generates a new type of $\mathcal{PT}$ symmetry, dubbed the non-Bloch $\mathcal{PT}$ symmetry, featuring unique properties such as high sensitivity to the boundary condition. Despite its relevance to a wide range of non-Hermitian lattice systems, a general theory is still lacking for this generic phenomenon even in one spatial dimension. Here, we uncover the geometric mechanism of non-Bloch $\mathcal{PT}$ symmetry and its breaking. We find that non-Bloch $\mathcal{PT}$ symmetry breaking occurs by the formation of cusps in the generalized Brillouin zone (GBZ). Based on this geometric understanding, we propose an exact formula that efficiently determines the breaking threshold. Moreover, we predict a new type of spectral singularities associated with the symmetry breaking, dubbed non-Bloch van Hove singularity, whose physical mechanism fundamentally differs from their Hermitian counterparts. This singularity is experimentally observable in linear responses.

DOI: 10.1103/PhysRevLett.132.050402

Introduction.—Parity-time ($\mathcal{PT}$) symmetry is one of the central concepts in non-Hermitian physics [1–5]. A $\mathcal{PT}$-symmetric Hamiltonian enjoys a real-valued spectrum when the non-Hermiticity is below a certain threshold. Above this threshold, the symmetry-protected reality breaks down. This real-to-complex transition has been associated with the exceptional points (EP) where a pair of eigenstates coalesce [6–10]. The unique properties of $\mathcal{PT}$ symmetry and EP have inspired numerous explorations on various experimental platforms [11–19].

Recently, the non-Hermitian skin effect (NHSE) has been realized as a general mechanism for achieving $\mathcal{PT}$ symmetry and therefore real spectrums [20–26]. NHSE refers to the phenomenon that the eigenstates of non-Hermitian systems are squeezed to the boundary under open boundary condition (OBC), which causes strong sensitivity of the spectrum to boundary conditions [27–38]. Its quantitative description requires a non-Bloch band theory that generalizes the concept of Brillouin zone [27,39–45]. In the presence of NHSE, it is possible to have an entirely real spectrum under OBC, in sharp contrast to that under periodic boundary condition (PBC), which is always complex [46,47]. That the real spectrum can only be maintained under OBC is known as *non-Bloch $\mathcal{PT}$ symmetry* [20–22], which is crucial in the experimental detection of non-Bloch band topology [33,48]. Recent experiments have confirmed the non-Bloch $\mathcal{PT}$ symmetry breaking transitions, i.e., the real-to-complex transitions of the OBC spectrum [22,23].

The $\mathcal{PT}$ symmetry breaking in Bloch bands originates exclusively from the Bloch Hamiltonian being defective at certain wave vectors [11,14,49–51]. The non-Bloch $\mathcal{PT}$ symmetry breaking, however, must have an entirely different mechanism. One of the clear evidences is that the non-Bloch $\mathcal{PT}$ breaking can occur in single-band systems. In contrast, the Bloch $\mathcal{PT}$ breaking is strictly prohibited in a single-band system because its Bloch Hamiltonian, as a complex number, can never be defective. It is the purpose of this paper to unveil the mechanism of non-Bloch $\mathcal{PT}$ breaking.

We uncover a geometric origin of non-Bloch $\mathcal{PT}$ symmetry breaking and formulate a coherent theory that enables efficient computation of the $\mathcal{PT}$ breaking threshold in one dimension (1D). Specifically, the geometric object we will focus on is the generalized Brillouin zone (GBZ), which can be determined through 1D non-Bloch band theory [27,39]. Because of its noncircular shape, the GBZ can possibly have intriguing cusp singularities [39,52], yet their physical significance remains elusive. Our work starts from the observation that these singularities underlie the non-Bloch $\mathcal{PT}$ symmetry breaking. Our main results include (i) The cusps on a GBZ are responsible for the non-Bloch $\mathcal{PT}$ symmetry breaking. (ii) A concise formula is found for the $\mathcal{PT}$ breaking threshold that does not require calculating the energy spectrum or GBZ. (iii) The transition point of non-Bloch $\mathcal{PT}$ symmetry breaking represents a new type of divergence in the density of states (DOS), which we call the non-Bloch van Hove singularity.

Geometric origin.—Non-Bloch $\mathcal{PT}$ symmetry breaking refers to the real-to-complex transition of the OBC spectrum in non-Hermitian bands. We first attempt to gain some intuitions about this transition from a concrete example.

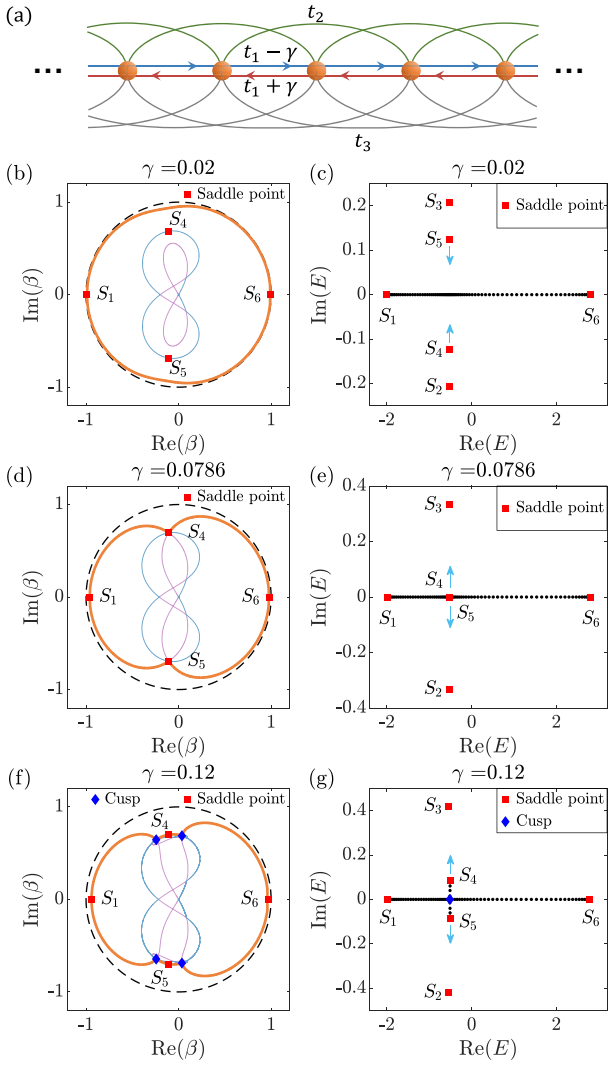

FIG. 1. (a) The real-space hopping in the model of Eq. (1). (b)–(g) The transition of the GBZ and the energy spectrum in a representative breaking process, with parameters $t_1 = 1$, $t_2 = t_3 = 0.2$. The energy spectrums are obtained by diagonalizing the real-space Hamiltonian under OBC with $L = 80$. (b),(c) The $\mathcal{PT}$-exact phase with $\gamma = 0.02$; (d),(e) the transition point with $\gamma = 0.0786$; and (f),(g) the $\mathcal{PT}$-broken phase with $\gamma = 0.12$. In (b),(d),(f) the black dashed loop is the BZ, the orange loop is the GBZ, and other branches in the aGBZ are labeled with different colors. S_2 and S_3 in (c),(e),(g) are outside the plot region of (b),(d),(f).

A simple model that includes all the ingredients of our interest has the Bloch Hamiltonian:

$$H(k) = 2t_1 \cos k + 2t_2 \cos 2k + 2t_3 \cos 3k + 2i\gamma \sin k. \quad (1)$$

Its real-space hopping is illustrated in Fig. 1(a). The real-space Hamiltonian H has real matrix elements and hence obeys the (generalized) $\mathcal{PT}$ symmetry $\mathcal{K}H\mathcal{K} = H$, where $\mathcal{K}$ is the complex conjugate operator [2]. The (generalized) $\mathcal{PT}$ symmetry is essential for obtaining a robust non-Bloch $\mathcal{PT}$-exact phase (i.e., a parameter region with nonzero measure where OBC spectrums are purely real).

The standard approach to obtain the OBC spectrum of the model in Eq. (1) is to use the non-Bloch band theory, which takes into account the NHSE [27,39]. In this approach, the Bloch Hamiltonian is generalized to the complex plane $H(\beta) \equiv H(k)|_{e^{ik}\to\beta}$, dubbed non-Bloch Hamiltonian. The OBC spectrum is given by $H(\beta)$, where β is taken from the GBZ, rather than the Brillouin zone (BZ). The GBZ is a curve determined by the GBZ equation $|\beta_i(E)| = |\beta_{i+1}(E)|$, where $\beta_i(E)$ and $\beta_{i+1}(E)$ are the middle two among all roots of the characteristic function $f(E,\beta) = \det[H(\beta) - E\mathbb{1}] = 0$ sorted by their moduli [53]. Thus, the decay factor (also known as the inverse skin depth) of a non-Hermitian skin mode is given by $\ln|\beta|$ with $\beta \in$ GBZ. Numerically, an efficient approach to solve the GBZ is to first obtain the so-called auxiliary GBZ (aGBZ) [42], which comprises a bunch of curves satisfying $|\beta_i(E)| = |\beta_j(E)|$ for any $i \neq j$. Then the GBZ comes as a subset of the aGBZ by further choosing the indices of these roots with equal moduli.

In Fig. 1, we demonstrate a paradigmatic non-Bloch $\mathcal{PT}$ transition within the model Eq. (1). With increasing γ, the OBC spectrum changes from entirely real to partially complex. Moreover, the continuity of GBZ changes saliently before and after the transition point. The GBZ is completely smooth in the $\mathcal{PT}$-exact phase [Fig. 1(b)], but becomes singular at several cusps when $\mathcal{PT}$ symmetry is broken [Fig. 1(f)]. Remarkably, the cusps appear exactly at the transition point [Fig. 1(d)].

At the same time, we mark *saddle points* that satisfy $f(E,\beta) = \partial_\beta f(E,\beta) = 0$ [20] by the red points in Fig. 1. Tracking their motions can help us understand the generation of GBZ cusps. A saddle point must reside on the aGBZ, but it may or may not be on the GBZ [42,54]. In Fig. 1(b), S_4 and S_5 reside on the aGBZ but not on the GBZ. However, as indicated in Figs. 1(d) and 1(f), they are merged into the GBZ at the transition point. For this to be possible, at the transition point the GBZ intersects with multiple branches of the aGBZ [Fig. 1(d)], which results in S_4 and S_5 being saddle points and GBZ cusps simultaneously.

To interpret the above observations, we parametrize the GBZ as $\beta = |\beta(\theta)|e^{i\theta}$. It suffices that a parametrization exists in a neighborhood of a given β. The derivative of the energy dispersion $E(\theta) = H(|\beta(\theta)|e^{i\theta})$ with respect to angle θ is

$$\frac{dE(\theta)}{d\theta} = \frac{\partial H(\beta)}{\partial \beta}\left(\frac{\partial|\beta(\theta)|}{\partial\theta}e^{i\theta} + i\beta\right). \quad (2)$$

The cusps correspond to discontinuous points of $\partial|\beta(\theta)|/\partial\theta$, and thus $dE(\theta)/d\theta$ is also discontinuous at the cusp unless $\partial_\beta H(\beta) = 0$. It is this discontinuity that accounts for the multiple branches of the spectrum on the

complex plane, and the branch point is just the cusp energy. This explains why the spectrum in the $\mathcal{PT}$-exact phase simply lies on the real axis [Fig. 1(c)], while it becomes complex and ramified in the $\mathcal{PT}$-broken phase [Fig. 1(g)]. In the critical cases [Figs. 1(d) and 1(e)], a cusp appears but the spectrum is still entirely real. This is only possible when these cusps are also saddle points satisfying $\partial_\beta H(\beta) = 0$ [56].

The above analysis indicates that the emergence of GBZ cusps is a geometric origin of non-Bloch $\mathcal{PT}$ symmetry breaking. The Supplemental Material [54] includes more examples that demonstrate this cusp mechanism, which can be generally formulated as follows:

(i) A $\mathcal{PT}$-symmetric lattice system has a smooth GBZ if it is in the non-Bloch $\mathcal{PT}$-exact phase.

(ii) If there are cusps on the GBZ, the system is either in the non-Bloch $\mathcal{PT}$-broken phase or at the $\mathcal{PT}$ transition point.

The proof of this result is given in [54]. It leverages a basic property of arbitrary non-Hermitian lattice systems with short-range hoppings, namely, the analyticity of the characteristic polynomial $f(E,\beta)$ with respect to β and E.

Simple formula for the breaking threshold.—In addition to the geometric origin, another piece of information conveyed by the model Eq. (1) is that its $\mathcal{PT}$ transition is characterized by the motion of saddle-point energies. With increasing non-Hermiticity, the energies of S_4 and S_5 move upward and downward, respectively [Figs. 1(c), 1(e), and 1(g)]. Notably, along with S_4 and S_5 being merged into the GBZ [Fig. 1(d)], their energies coalesce on the real axis at the transition point [Fig. 1(e)]. For a single-band model with non-Bloch Hamiltonian $H(\beta) = \sum_{n=-l}^{r} h_n \beta^n$, such a coalescence is described by

$$H(\beta_{s,i}) = H(\beta_{s,j}) \in \mathbb{R}, \tag{3}$$

where $\beta_{s,i}$ and $\beta_{s,j}$ are two different saddle points on the GBZ, satisfying $\partial_\beta H(\beta) = 0$. We will demonstrate that the condition Eq. (3) serves as an efficient criterion for determining the non-Bloch $\mathcal{PT}$ breaking threshold.

We shall rephrase Eq. (3) in two steps to make its identification more feasible. First, we utilize a mathematical concept called *resultant* to search for any degeneracy of saddle-point energies, i.e., $H(\beta_{s,i}) = H(\beta_{s,j})$ with $i \neq j$. Then, we locate the parameter values that fulfill the condition Eq. (3) by examining both the reality of the degenerate energies and whether the associated saddle points belong to the GBZ. Here, the resultant is defined to identify whether two given polynomials have a common root [57]. For example, the resultant $\mathrm{Res}_x[x-a, x-b] = a-b$ equals zero if and only if the roots $x = a$ and $x = b$ are degenerate. Recalling that the saddle points are exactly the common roots of $f(E,\beta) = H(\beta) - E = 0$ and $\partial_\beta f(E,\beta) = \partial_\beta H(\beta) = 0$, saddle-point energies $E_{s,i} = H(\beta_{s,i})$ can be directly found by eliminating β, which results in

$$g(E) = \mathrm{Res}_\beta\left[\tilde{f}(E,\beta), \partial_\beta \tilde{f}(E,\beta)\right] = 0, \tag{4}$$

where $\tilde{f}(E,\beta) = \beta^l f(E,\beta)$ is used to avoid negative powers of β. The roots of $g(E) = 0$ are exactly all the saddle-point energies $E_{s,i}$, i.e., $g(E) \propto \prod_i (E - E_{s,i})$. On the other hand, the coalescence condition Eq. (3) suggests at least a pair of $E_{s,i}$ are degenerate, which is thus equivalent to $\partial_E g(E) = 0$. Therefore, the parameters with degenerate saddle-point energies can be solved from

$$\mathrm{Res}_E[g(E), \partial_E g(E)] = 0. \tag{5}$$

A standard procedure to derive the above resultants is through the Sylvester matrix [54].

When we consider γ variable and other parameters fixed, $\mathrm{Res}_E[g(E), \partial_E g(E)]$ is nothing but a polynomial of γ. We are now in a place to tell which root of this polynomial truly contributes to the coalescence described by Eq. (3). In practice, the desired root is recognized under the following procedure. We insert γ obtained from Eq. (5) back into Eq. (4) to find out the degenerate energies E_s. Then, we solve and sort the roots of $f(E_s,\beta) = \sum_{n=-l}^{r} h_n \beta^n - E_s = 0$ as $|\beta_1(E_s)| \leq \ldots \leq |\beta_{l+r}(E_s)|$. Moreover, since Eq. (5) is equivalent to the existence of a pair of saddle points with the same energy, we can find two roots $\beta_{s,i}$ and $\beta_{s,j}$ from $f(E_s,\beta) = \partial_\beta f(E_s,\beta) = 0$. Finally, according to the GBZ equation and Eq. (3), the $\mathcal{PT}$ breaking threshold is determined by selecting those roots of Eq. (5) that fulfill the conditions $\mathrm{Im}E_s = 0$ and $|\beta_{s,i}| = |\beta_{s,j}| = |\beta_l(E_s)| = |\beta_{l+1}(E_s)|$ [58].

So far, we have built up a systematic algebraic method for determining the breaking threshold, the power of which lies in the fact that we are able to find the phase boundary without diagonalizing the real-space Hamiltonian or calculating the complete GBZ. In the Supplemental Material [54], we explicitly illustrate how to conduct this method step by step for the model Eq. (1) with $t_2 = t_3 = 0$. For more general parameters (t_2, t_3 nonzero), filtering the roots of Eq. (5) with the GBZ equation is also accurate and effortless for determining the phase boundary. We demonstrate its results in Fig. 2: the boundary between $\mathcal{PT}$-exact and $\mathcal{PT}$-broken phases in the model Eq. (1) obtained via diagonalization agrees well with the one through proper selection of the roots of Eq. (5). The analytic method is, however, much more efficient and free of finite-size effects.

Not limited to single-band cases, on a non-Hermitian chain with $\mathcal{PT}$ symmetry, the generation of the first pair of complex conjugate saddle-point energies contained in the OBC spectrum inevitably involves a coalescence like Eq. (3). This process, whose transition point is predicted by the method introduced here, is experimentally detectable in wave-packet dynamics [20,22,23].

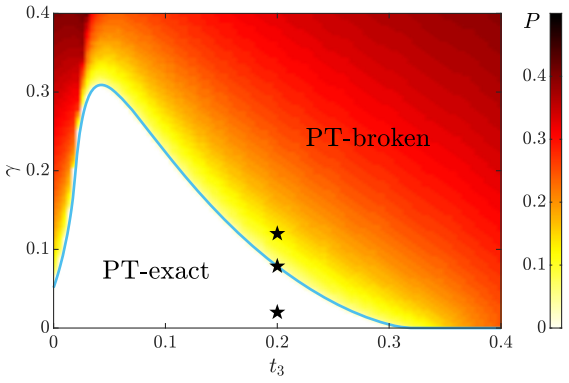

FIG. 2. The non-Bloch $\mathcal{PT}$ phase diagram of the model Eq. (1) with $t_1 = 1$, $t_2 = 0.2$. The blue line is the phase boundary determined by solving Eq. (5). The color map is a density plot for the proportion P of complex eigenvalues, obtained by counting the proportion of eigenenergies with $|\mathrm{Im}E| > 10^{-10}$. The eigenenergies are obtained by diagonalizing an OBC Hamiltonian of length $L = 200$. The three black stars mark the parameters used in Fig. 1.

Non-Bloch van Hove singularity.—As previously mentioned, at the $\mathcal{PT}$ transition point [Figs. 1(d) and 1(e)], there exist saddle points on the GBZ that are also cusps. This is a hallmark of the geometric origin of $\mathcal{PT}$-breaking transitions. We shall elucidate the observable consequences of these cusps by examining the non-Hermitian Green's function, defined as $G(E) = (E - H)^{-1}$, where H is the OBC Hamiltonian generated by the Bloch Hamiltonian [e.g., Eq. (1)]. Practically, $G(E)$ can be measured through frequency-dependent linear responses on various platforms such as topolectrical circuits [32,59], scattering processes [60], and open quantum systems [61].

In the $\mathcal{PT}$-exact phase, we define the DOS along the real axis by $\rho(E) = (\pi L)^{-1}\mathrm{Im}\mathrm{Tr}[G(E + i0^+)]$, or, equivalently, $\rho(E) = L^{-1}\sum_{i=1}^{L}\delta(E - E_i)$, where E and the eigenenergies E_i are all real. When the system size L goes to infinity, the summation over all eigenenergies becomes an integral along GBZ [54,61]. Thus, we have

$$\rho(E) = \frac{1}{2\pi}\sum_{\beta(E)\in\mathrm{GBZ}}\left|\mathrm{Im}\left[\frac{1}{\beta\partial_\beta H(\beta)}\right]_{\beta=\beta(E)}\right|, \qquad (6)$$

which is a natural extension of the well-known formula $\rho(E) = (1/2\pi)\sum_{E(k)=E}|\partial E(k)/\partial k|^{-1}$ for the Hermitian case.

According to Eq. (6), the DOS is divergent at any saddle point on the GBZ. From Figs. 3(a) and 3(b), we find that the DOS near $E_s \approx -0.5096$ increases and eventually becomes divergent at the transition point. This divergence is analogous to the van Hove singularity in Hermitian systems, but is induced by the singular shape of the GBZ, which is unique to systems with NHSE. At the non-Bloch $\mathcal{PT}$ symmetry breaking point, the cusps, which are at the same time saddle points, are responsible for the divergence at E_s. Thus, we coin for this divergence the term *non-Bloch van Hove singularity.*

Quantitatively, the asymptotic behavior of the DOS near a non-Bloch van Hove singularity can be inferred from Eq. (6). Near a saddle point E_s, $|\beta\partial_\beta H(\beta)|$ behaves like $|E - E_s|^\alpha$. Inserting this back into Eq. (6), we find that the DOS is locally $\rho(E) \sim |E - E_s|^{-\alpha}$. Generally, the exponent α for a kth order saddle point (satisfying $H(\beta) - E = \partial_\beta H(\beta) = \ldots = \partial_\beta^{k-1}H(\beta) = 0$) is $\alpha = 1 - 1/k$. Our model with nonzero t_3 gives $\alpha = 1/2$, which is in accordance with the numerical fitting $\rho \sim |E - E_s|^{-1/2}$ shown in Fig. 3(a). Interestingly, in our model with $t_3 = 0$, two second-order saddle points are merged into one third-order saddle point at the transition point of non-Bloch $\mathcal{PT}$ breaking. According to $\alpha = 1 - 1/k$, this also implies that the exponent suddenly changes at the transition point. More details about the jump of α can be found in [54].

Beyond divergent DOS, the non-Bloch van Hove singularity also manifests itself in the off-diagonal elements of $G(E)$. On a finite chain with length L, the end-to-end Green's functions exhibit exponential growth or decay, represented as $|G_{L1}(E)| \sim \alpha_r(E)^L$ and $|G_{1L}(E)| \sim \alpha_l(E)^L$. The two scaling factors $\alpha_r(E)$ and $\alpha_l(E)$ can be

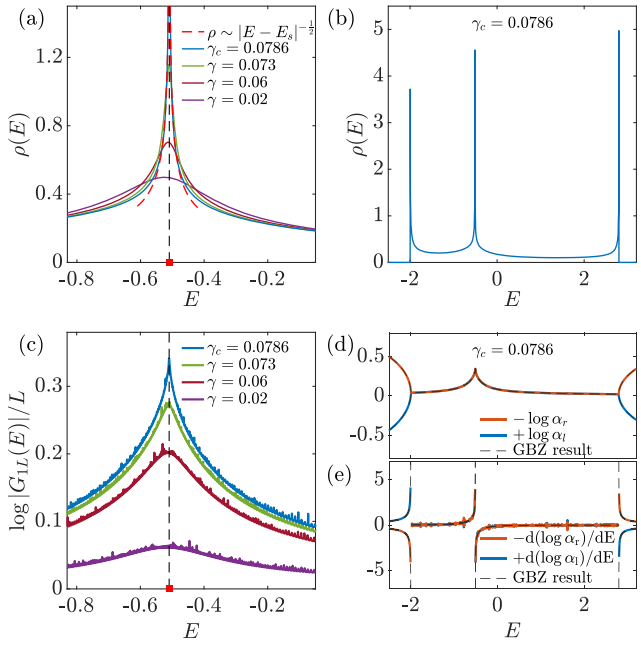

FIG. 3. Non-Bloch van Hove singularity. (a) The DOS in the non-Bloch $\mathcal{PT}$-exact phase. (b) A full profile of DOS at the transition point $\gamma_c = 0.0786$. (c),(d) The frequency dependence of $\log\alpha_l(E) = \log|G_{1L}(E)|/L$. (e) $\mathrm{d}(\log\alpha_{l,r}(E))/\mathrm{d}E$ for the scaling factors in (d). The dashed lines in (d),(e) mark the theoretical predictions based on GBZ. To reduce data fluctuations due to finite-size effects, the $\alpha_{l,r}(E)$ in (d),(e) are obtained by fitting $\log|G_{1L}(E)|$ and $\log|G_{L1}(E)|$ with respect to the system size L. We fix $L = 500$ in (c) and take $L \in [100, 300]$ in (d),(e). The parameters are $t_1 = 1$, $t_2 = t_3 = 0.2$.

predicted using non-Bloch band theory [61,62]. For the model Eq. (1) with $t_3 \neq 0$, we have $\alpha_r(E) = |\beta_3(E)|$ and $\alpha_l(E) = |\beta_4(E)|^{-1}$, where $|\beta_{3,4}(E)|$ are the roots of $H(\beta) = E$ sorted as $|\beta_1(E)| \leq \ldots \leq |\beta_6(E)|$. When E belongs to the OBC spectrum, $\alpha_{r,l}(E)$ encode crucial information about GBZ. We find that the frequency dependence of $\alpha_{r,l}(E)$ exhibits a cusp precisely at the energy of the non-Bloch van Hove singularity [Figs. 3(c) and 3(d)]. This occurs concurrently with the emergence of GBZ cusps at the transition point. Furthermore, since these GBZ cusps are also saddle points, the nonsmoothness of $\alpha_{r,l}(E)$ stems from divergent $\mathrm{d}\alpha_{r,l}(E)/\mathrm{d}E$ [63] [Fig. 3(e)]. Practically, the divergence in $\mathrm{d}\alpha_{r,l}(E)/\mathrm{d}E$ signals extreme frequency sensitivity in the response to the input signal, which could potentially inspire designs of non-Hermitian sensors [64,65].

Conclusions.—We have presented a theory of non-Bloch $\mathcal{PT}$ symmetry breaking in one dimension, which not only explains its geometric origin but also provides an efficient formula for the threshold. Given the fact that the concept of GBZ has recently been generalized to non-Hermitian continuum systems [66–69] and disordered systems [70,71], it is an interesting direction to develop our theory in these contexts. Moreover, it is known that the threshold in higher dimensions universally approaches zero as the system size increases [72]. In view of the latest progress on higher-dimensional GBZ [73,74], our theory can have implications for $\mathcal{PT}$ symmetry in higher dimensions. For example, since the non-Bloch van Hove singularities are tied to the non-Bloch $\mathcal{PT}$ symmetry breaking in one dimension, their proliferation in higher dimensions may be responsible for the universal thresholdless behavior, which is left for future studies. Back to the 1D cases that are experimentally most convenient, our predictions can be verified on various state-of-the-art platforms such as cold atom [75,76] and quantum optics systems [22].

This work is supported by NSFC under Grant No. 12125405.

*songfeiphys@gmail.com

[1] C. M. Bender and S. Boettcher, Real spectra in non-Hermitian Hamiltonians having $\mathcal{PT}$ symmetry, Phys. Rev. Lett. **80**, 5243 (1998).

[2] C. M. Bender, M. V. Berry, and A. Mandilara, Generalized $\mathcal{PT}$ symmetry and real spectra, J. Phys. A **35**, L467 (2002).

[3] C. M. Bender, Making sense of non-Hermitian Hamiltonians, Rep. Prog. Phys. **70**, 947 (2007).

[4] A. Mostafazadeh, Pseudo-Hermiticity versus $\mathcal{PT}$-symmetry: The necessary condition for the reality of the spectrum of a non-Hermitian Hamiltonian, J. Math. Phys. (N.Y.) **43**, 205 (2002).

[5] A. Mostafazadeh, Pseudo-Hermiticity versus $\mathcal{PT}$-symmetry. II. A complete characterization of non-Hermitian Hamiltonians with a real spectrum, J. Math. Phys. (N.Y.) **43**, 2814 (2002).

[6] Ş. K. Özdemir, S. Rotter, F. Nori, and L. Yang, Parity-time symmetry and exceptional points in photonics, Nat. Mater. **18**, 783 (2019).

[7] R. El-Ganainy, K. G. Makris, M. Khajavikhan, Z. H. Musslimani, S. Rotter, and D. N. Christodoulides, Non-Hermitian physics and $\mathcal{PT}$ symmetry, Nat. Phys. **14**, 11 (2018).

[8] M.-A. Miri and A. Alù, Exceptional points in optics and photonics, Science **363**, eaar7709 (2019).

[9] W. Heiss, Exceptional points of non-Hermitian operators, J. Phys. A **37**, 2455 (2004).

[10] M. V. Berry, Physics of non-Hermitian degeneracies, Czech. J. Phys. **54**, 1039 (2004).

[11] K. G. Makris, R. El-Ganainy, D. N. Christodoulides, and Z. H. Musslimani, Beam dynamics in $\mathcal{PT}$ symmetric optical lattices, Phys. Rev. Lett. **100**, 103904 (2008).

[12] A. Guo, G. J. Salamo, D. Duchesne, R. Morandotti, M. Volatier-Ravat, V. Aimez, G. A. Siviloglou, and D. N. Christodoulides, Observation of $\mathcal{PT}$-symmetry breaking in complex optical potentials, Phys. Rev. Lett. **103**, 093902 (2009).

[13] Z. Lin, H. Ramezani, T. Eichelkraut, T. Kottos, H. Cao, and D. N. Christodoulides, Unidirectional invisibility induced by $\mathcal{PT}$-symmetric periodic structures, Phys. Rev. Lett. **106**, 213901 (2011).

[14] A. Regensburger, C. Bersch, M.-A. Miri, G. Onishchukov, D. N. Christodoulides, and U. Peschel, Parity–time synthetic photonic lattices, Nature (London) **488**, 167 (2012).

[15] S. Bittner, B. Dietz, U. Günther, H. L. Harney, M. Miski-Oglu, A. Richter, and F. Schäfer, $\mathcal{PT}$-symmetry and spontaneous symmetry breaking in a microwave billiard, Phys. Rev. Lett. **108**, 024101 (2012).

[16] H. Hodaei, M.-A. Miri, M. Heinrich, D. N. Christodoulides, and M. Khajavikhan, Parity-time–symmetric microring lasers, Science **346**, 975 (2014).

[17] L. Feng, Z. J. Wong, R.-M. Ma, Y. Wang, and X. Zhang, Single-mode laser by parity-time symmetry breaking, Science **346**, 972 (2014).

[18] R. Fleury, D. Sounas, and A. Alù, An invisible acoustic sensor based on parity-time symmetry, Nat. Commun. **6**, 5905 (2015).

[19] H. Hodaei, A. U. Hassan, S. Wittek, H. Garcia-Gracia, R. El-Ganainy, D. N. Christodoulides, and M. Khajavikhan, Enhanced sensitivity at higher-order exceptional points, Nature (London) **548**, 187 (2017).

[20] S. Longhi, Probing non-Hermitian skin effect and non-Bloch phase transitions, Phys. Rev. Res. **1**, 023013 (2019).

[21] S. Longhi, Non-Bloch $\mathcal{PT}$ symmetry breaking in non-Hermitian photonic quantum walks, Opt. Lett. **44**, 5804 (2019).

[22] L. Xiao, T. Deng, K. Wang, Z. Wang, W. Yi, and P. Xue, Observation of non-Bloch parity-time symmetry and exceptional points, Phys. Rev. Lett. **126**, 230402 (2021).

[23] S. Weidemann, M. Kremer, S. Longhi, and A. Szameit, Topological triple phase transition in non-Hermitian Floquet quasicrystals, Nature (London) **601**, 354 (2022).

[24] R. Yang, J. W. Tan, T. Tai, J. M. Koh, L. Li, S. Longhi, and C. H. Lee, Designing non-Hermitian real spectra through electrostatics, Sci. Bull. **67**, 1865 (2022).

[25] B. Zhang, Q. Li, X. Zhang, and C. H. Lee, Real non-Hermitian energy spectra without any symmetry, Chin. Phys. B **31**, 070308 (2022).

[26] Q.-B. Zeng and R. Lü, Real spectra and phase transition of skin effect in nonreciprocal systems, Phys. Rev. B **105**, 245407 (2022).

[27] S. Yao and Z. Wang, Edge states and topological invariants of non-Hermitian systems, Phys. Rev. Lett. **121**, 086803 (2018).

[28] S. Yao, F. Song, and Z. Wang, Non-Hermitian Chern bands, Phys. Rev. Lett. **121**, 136802 (2018).

[29] F. K. Kunst, E. Edvardsson, J. C. Budich, and E. J. Bergholtz, Biorthogonal bulk-boundary correspondence in non-Hermitian systems, Phys. Rev. Lett. **121**, 026808 (2018).

[30] C. H. Lee and R. Thomale, Anatomy of skin modes and topology in non-Hermitian systems, Phys. Rev. B **99**, 201103(R) (2019).

[31] V. M. Martinez Alvarez, J. E. Barrios Vargas, and L. E. F. Foa Torres, Non-Hermitian robust edge states in one dimension: Anomalous localization and eigenspace condensation at exceptional points, Phys. Rev. B **97**, 121401(R) (2018).

[32] T. Helbig, T. Hofmann, S. Imhof, M. Abdelghany, T. Kiessling, L. Molenkamp, C. Lee, A. Szameit, M. Greiter, and R. Thomale, Generalized bulk–boundary correspondence in non-Hermitian topolectrical circuits, Nat. Phys. **16**, 747 (2020).

[33] L. Xiao, T. Deng, K. Wang, G. Zhu, Z. Wang, W. Yi, and P. Xue, Non-Hermitian bulk-boundary correspondence in quantum dynamics, Nat. Phys. **16**, 761 (2020).

[34] A. Ghatak, M. Brandenbourger, J. van Wezel, and C. Coulais, Observation of non-Hermitian topology and its bulk–edge correspondence in an active mechanical metamaterial, Proc. Natl. Acad. Sci. U.S.A. **117**, 29561 (2020).

[35] S. Weidemann, M. Kremer, T. Helbig, T. Hofmann, A. Stegmaier, M. Greiter, R. Thomale, and A. Szameit, Topological funneling of light, Science **368**, 311 (2020).

[36] T. Hofmann, T. Helbig, F. Schindler, N. Salgo, M. Brzezińska, M. Greiter, T. Kiessling, D. Wolf, A. Vollhardt, A. Kabaši, C. H. Lee, A. Bilušić, R. Thomale, and T. Neupert, Reciprocal skin effect and its realization in a topolectrical circuit, Phys. Rev. Res. **2**, 023265 (2020).

[37] E. J. Bergholtz, J. C. Budich, and F. K. Kunst, Exceptional topology of non-Hermitian systems, Rev. Mod. Phys. **93**, 015005 (2021).

[38] Y. Ashida, Z. Gong, and M. Ueda, Non-Hermitian physics, Adv. Phys. **69**, 249 (2020).

[39] K. Yokomizo and S. Murakami, Non-Bloch band theory of non-Hermitian systems, Phys. Rev. Lett. **123**, 066404 (2019).

[40] K. Yokomizo and S. Murakami, Non-Bloch band theory and bulk–edge correspondence in non-Hermitian systems, Prog. Theor. Exp. Phys. **2020**, 12A102 (2020).

[41] Z. Wang, Non-Bloch band theory and beyond, in *Memorial Volume for Shoucheng Zhang* (World Scientific, Singapore, 2021), pp. 365–387.

[42] Z. Yang, K. Zhang, C. Fang, and J. Hu, Non-Hermitian bulk-boundary correspondence and auxiliary generalized Brillouin zone theory, Phys. Rev. Lett. **125**, 226402 (2020).

[43] S. Longhi, Non-Bloch-band collapse and chiral Zener tunneling, Phys. Rev. Lett. **124**, 066602 (2020).

[44] K. Kawabata, N. Okuma, and M. Sato, Non-Bloch band theory of non-Hermitian Hamiltonians in the symplectic class, Phys. Rev. B **101**, 195147 (2020).

[45] T.-S. Deng and W. Yi, Non-Bloch topological invariants in a non-Hermitian domain wall system, Phys. Rev. B **100**, 035102 (2019).

[46] K. Zhang, Z. Yang, and C. Fang, Correspondence between winding numbers and skin modes in non-Hermitian systems, Phys. Rev. Lett. **125**, 126402 (2020).

[47] N. Okuma, K. Kawabata, K. Shiozaki, and M. Sato, Topological origin of non-Hermitian skin effects, Phys. Rev. Lett. **124**, 086801 (2020).

[48] K. Wang, T. Li, L. Xiao, Y. Han, W. Yi, and P. Xue, Detecting non-Bloch topological invariants in quantum dynamics, Phys. Rev. Lett. **127**, 270602 (2021).

[49] S. Longhi, Bloch oscillations in complex crystals with $\mathcal{PT}$ symmetry, Phys. Rev. Lett. **103**, 123601 (2009).

[50] N. Bender, H. Li, F. M. Ellis, and T. Kottos, Wave-packet self-imaging and giant recombinations via stable Bloch-Zener oscillations in photonic lattices with local pt symmetry, Phys. Rev. A **92**, 041803(R) (2015).

[51] A. Stegmaier, S. Imhof, T. Helbig, T. Hofmann, C. H. Lee, M. Kremer, A. Fritzsche, T. Feichtner, S. Klembt, S. Höfling *et al.*, Topological defect engineering and $\mathcal{PT}$ symmetry in non-Hermitian electrical circuits, Phys. Rev. Lett. **126**, 215302 (2021).

[52] K. Yokomizo and S. Murakami, Topological semimetal phase with exceptional points in one-dimensional non-Hermitian systems, Phys. Rev. Res. **2**, 043045 (2020).

[53] Sorting all roots by their moduli, $\beta_i(E)$ and $\beta_{i+1}(E)$ are the ith and the $(i+1)$-th roots, respectively, where i is the order of the pole of the Laurent polynomial $f(E,\beta)$ at $\beta=0$. For example, the model Eq. (1) with nonzero t_3 has the index $i=3$.

[54] See Supplemental Material at http://link.aps.org/supplemental/10.1103/PhysRevLett.132.050402 for technical details of our theory and more supporting examples, which also includes Ref. [55].

[55] A. Böttcher and S. M. Grudsky, *Spectral Properties of Banded Toeplitz Matrices* (SIAM, Philadelphia, 2005).

[56] The reality of the spectrum guarantees $d_\theta \mathrm{Im}E(\theta)=0$. Meanwhile, one can derive $d_\theta \mathrm{Im}E(\theta)=\mathrm{Re}[\beta\partial_\beta H(\beta)]+\mathrm{Im}[\beta\partial_\beta H(\beta)]\partial_\theta \log|\beta(\theta)|$ from Eq. (2). For a cusp $\beta_c=|\beta(\theta_c)|e^{i\theta_c}\in\mathrm{GBZ}$ where $(\partial|\beta(\theta)|/\partial\theta)_{\theta\to\theta_c^-}\neq(\partial|\beta(\theta)|/\partial\theta)_{\theta\to\theta_c^+}$, it follows that $\mathrm{Re}[\beta\partial_\beta H(\beta)]=\mathrm{Im}[\beta\partial_\beta H(\beta)]=0$. Since GBZ does not pass $\beta=0$ in general, we conclude that β_c should be a saddle point.

[57] S. Lang, *Algebra* (Springer, New York, 2002).

[58] Numerically, $|\beta|=|\beta'|$ is verified as $||\beta|-|\beta'||<\epsilon$, where we take ϵ to be 10^{-5}.

[59] L. Li, S. Mu, C. H. Lee, and J. Gong, Quantized classical response from spectral winding topology, Nat. Commun. **12**, 5294 (2021).

[60] H.-G. Zirnstein, G. Refael, and B. Rosenow, Bulk-boundary correspondence for non-Hermitian Hamiltonians via Green functions, Phys. Rev. Lett. **126**, 216407 (2021).

[61] W.-T. Xue, M.-R. Li, Y.-M. Hu, F. Song, and Z. Wang, Simple formulas of directional amplification from non-Bloch band theory, Phys. Rev. B **103**, L241408 (2021).
[62] Y.-M. Hu and Z. Wang, Green's functions of multiband non-Hermitian systems, Phys. Rev. Res. **5**, 043073 (2023).
[63] We notice that $\mathrm{d}\alpha_{r,l}(E)/\mathrm{d}E$ remains finite on one side of the left or right band edge. As explained in the Sec. II of [54], this is closely related to the fact that the saddle points $S_{1,6}$ shown in Fig. 1(d), which contribute the energies of two band edges, are not cusps.
[64] J. C. Budich and E. J. Bergholtz, Non-Hermitian topological sensors, Phys. Rev. Lett. **125**, 180403 (2020).
[65] A. McDonald and A. A. Clerk, Exponentially-enhanced quantum sensing with non-Hermitian lattice dynamics, Nat. Commun. **11**, 5382 (2020).
[66] S. Longhi, Non-Hermitian skin effect beyond the tight-binding models, Phys. Rev. B **104**, 125109 (2021).
[67] S. Guo, C. Dong, F. Zhang, J. Hu, and Z. Yang, Theoretical prediction of a non-Hermitian skin effect in ultracold-atom systems, Phys. Rev. A **106**, L061302 (2022).
[68] K. Yokomizo, T. Yoda, and S. Murakami, Non-Hermitian waves in a continuous periodic model and application to photonic crystals, Phys. Rev. Res. **4**, 023089 (2022).
[69] Y.-M. Hu, Y.-Q. Huang, W.-T. Xue, and Z. Wang, Non-Bloch band theory for non-Hermitian continuum systems, arXiv:2310.08572.
[70] Z.-Q. Zhang, H. Liu, H. Liu, H. Jiang, and X. Xie, Bulk-boundary correspondence in disordered non-Hermitian systems, Sci. Bull. **68**, 157 (2023).
[71] H. Liu, M. Lu, Z.-Q. Zhang, and H. Jiang, Modified generalized Brillouin zone theory with on-site disorder, Phys. Rev. B **107**, 144204 (2023).
[72] F. Song, H.-Y. Wang, and Z. Wang, Non-Bloch pt symmetry: Universal threshold and dimensional surprise, in *A Festschrift in Honor of the CN Yang Centenary: Scientific Papers* (World Scientific, Singapore, 2022), pp. 299–311.
[73] H.-Y. Wang, F. Song, and Z. Wang, Amoeba formulation of the non-Hermitian skin effect in higher dimensions, arXiv:2212.11743.
[74] H. Jiang and C. H. Lee, Dimensional transmutation from non-Hermiticity, Phys. Rev. Lett. **131**, 076401 (2023).
[75] J. Li, A. K. Harter, J. Liu, L. de Melo, Y. N. Joglekar, and L. Luo, Observation of parity-time symmetry breaking transitions in a dissipative Floquet system of ultracold atoms, Nat. Commun. **10**, 855 (2019).
[76] W. Gou, T. Chen, D. Xie, T. Xiao, T.-S. Deng, B. Gadway, W. Yi, and B. Yan, Tunable nonreciprocal quantum transport through a dissipative Aharonov-Bohm ring in ultracold atoms, Phys. Rev. Lett. **124**, 070402 (2020).